JOURNAL OF THERMOPHYSICS AND HEAT TRANSFER
Vol. 10, No. 4, October–December 1996

Radiative Emission from the Simulated Shock Layer of the Huygens Probe

Chung Sik Park* and Daniel Bershader†
Stanford University, Stanford, California 94305
and
Chul Park‡
NASA Ames Research Center, Moffett Field, California 94035-1000

An investigation has been conducted to determine the effect of nonequilibrium flow on the shock-layer radiation and radiative heat flux to the surface of the Huygens probe. The Huygens probe will enter the Titan atmosphere at a speed of 6 km/s in the spring of 2003. The shock-tube facility at Stanford University was used to generate high-temperature gas behind strong shocks advancing into a simulated Titan atmosphere. Conditions behind the shock approximate those in the Huygens forebody shock layer. Spectroscopic techniques have been used to measure thermophysical quantities of the high-temperature gas. A numerical code has been developed using a three-temperature model to generate one-dimensional flowfield solutions for comparison with these data. Agreement between the two methods has led to further confidence in the predicted radiative heat transfer magnitude in the probe stagnation region.

Nomenclature

A = Einstein coefficient
C_D = drag coefficient
C_L = lift coefficient
C_M = moment coefficient
c = continuum state
E = spontaneous emission
E_λ = spontaneous emission spectrum
I_λ = specific intensity
i = ith electronic state
K = excitation rate coefficient
l = optical path length
N = number density
P = pressure
Q = partition function, Eq. (2)
Qr = heat flux, Eq. (7)
T = temperature
V = velocity
y = distance behind the shock along the stagnation streamline
δ = shock standoff distance
λ = wavelength
ρ = density
τ = characteristic time

Subscripts
a = atom
E = electron–electronic
e = free electron
i = ith electronic state
r = radiative
s = condition right behind the shock
V = vibrational
∞ = freestream conditions

Received Feb. 20, 1996; revision received April 25, 1996; accepted for publication April 30, 1996.

*Research Assistant, Department of Aeronautics and Astronautics; currently Research Scientist, Thermosciences Institute, Moffett Field, CA 94035-1000. Member AIAA.

†Professor, Department of Aeronautics and Astronautics. Fellow AIAA.

‡Senior Research Scientist; currently Professor, Department of Aeronautics and Space Engineering, Tohoku University, Sendai, Japan. Fellow AIAA.

Introduction

THE joint ESA–NASA Cassini mission includes the Huygens probe that will penetrate the atmosphere of the Saturn moon Titan at hypersonic speeds of around 6 km/s. Data obtained from the Pioneer flyby indicate that the Titan atmosphere contains about 97% N_2, 3% CH_4, a small amount of Ar and H_2, as well as thin smog-like hazes of hydrocarbons. Titan is of scientific interest because the conditions of Titan may be similar to that of primitive Earth. Because of the high-entry velocity, the probe will meet a severe radiative aerothermodynamic environment upon further atmospheric penetration. The temperature behind the shock is high enough to ionize some component species, as well as dissociate the molecular constituents. Also, because of the high temperature and low pressure, we can expect a nonequilibrium phenomena in the flowfield around the probe. The radiative heat transfer to the capsule from the nonequilibrium shock layer was analyzed by Park,[1] considering all possible chemical reactions, but using one temperature model. As an extension of that previous work, we considered the flowfield to be characterized by three temperatures: 1) translational, 2) vibrational, and 3) electronic temperature, because of the relaxation phenomena. The species concentration as well as flow variables, such as temperature and pressure, was considered as a function of distance behind the shock. From that information of species concentration and flow variables, the radiation was calculated by a computer code, which is a modification of NEQAIR (nonequilibrium air radiation).[2]

A set of experiments was performed in the shock-tube laboratory. As the shock was flying by at 5.75 km/s, the time history of radiative emission was measured at different wavelengths to determine the absolute amount of radiation. The experimental data were compared with numerical analysis to validate and correct the modeling that was used in the numerical analysis. This one-dimensional analysis was extended to the calculation of radiative heating at the stagnation point of the probe. For this case, the one-dimensional approximation to the actual three-dimensional flowfield is appropriate.

Calculation of Flowfield

In previous work,[3] the thermophysical variables and species concentrations of high-temperature gas behind a strong normal shock were numerically calculated. In the calculation, a set of governing equations (species mass, momentum, total energy, vibrational energy, and electron–electronic energy) were integrated with respect to the distance behind the shock. Also, the chemical reactions were simultaneously solved with the governing equations by use of a three-temperature model. The results of the calculation are shown in Figs. 1–3. The freestream conditions in that calculation were 2 torr and 300 K, while the velocity of the freestream was 5.75 km/s and the composition mixture ratio of the freestream was 95.7% N_2, 0.3% H_2, 3% CH_4, and 1% Ar. In Fig. 1, the distributions of temperatures are shown as functions of distance behind the shock. The normalized pressure and density distributions are shown in Fig. 2. As seen in Fig. 3, new species were generated by the chemical reactions. The considered species in the calculation are N, N^+, N_2, N_2^+, CH, C, H, NH, CN, C_2, C^+, H^+, Ar, Ar^+, H_2, and CN^+. For convenience, only 10 species are shown in Fig. 3. The implicit trapezoidal scheme was used in the integration. More detailed information about the numerical scheme and chemical reaction rates are available in Ref. 4.

The accuracy of numerical calculation could be affected by grid size. To determine the optimum grid size, the integration was performed for various grid sizes. Then the grid size was determined such that the peak value of vibrational temperature and species number density change by 0.5%, whereas the grid size changes by a factor of 3 in both directions.

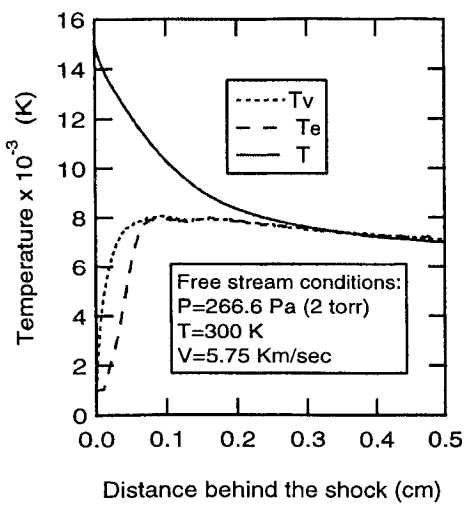

Fig. 1 Distribution of T, T_V, and T_E temperature as functions of the distance behind the shock.

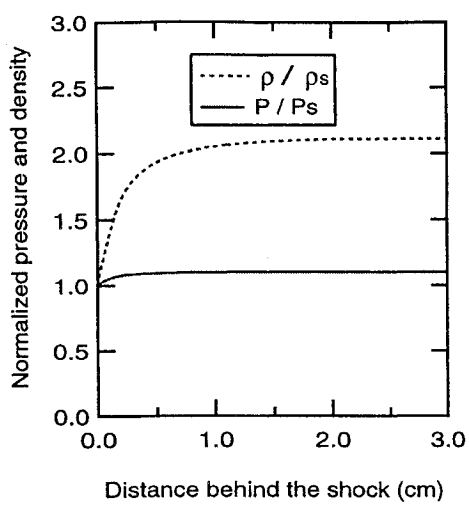

Fig. 2 Relaxation of normalized pressure and density behind the shock under the conditions of Fig. 1.

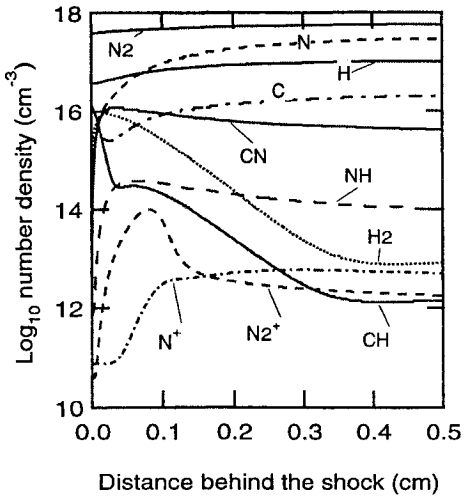

Fig. 3 Concentration of species behind the shock under the conditions of Fig. 1.

Master Equation

Using the values of physical variables and species number density of the high-temperature gas, the distribution of population among the electronic energy levels can be determined by solving the master equations. The electronic states of the species are excited and de-excited by the collisional and radiative processes, which determine the population distribution at a given time and location in the gas. With a given value of number density of the atoms N_a, electron number density N_e, electronic temperature T_e, and the number density of the ions N^+, the rate of change of number density of ith energy level can be expressed as

$$\frac{\partial N_i}{\partial t} = \sum_{j=1}^{m} K(i,j)N_jN_e + \sum_{j=1}^{m} A(i,j)N_j + K(c,i)N^+N_eN_e + A(c,i)N^+N_e - \sum_{j=1}^{m} K(j,i)N_jN_e - K(i,c)N_iN_e - \sum_{j=1}^{m} A(i,j)N_i - A(i,c)N_i \quad (1)$$

The first term in the right-hand side (RHS) of Eq. (1) is the rate of occurrence of transition from the initial state i to the final state j by the collisions between the atoms in ith electronic state and electrons. The fifth term represents the inverse process of first term. The value of $K(j,i)$ can be calculated by the principle of detailed balance, i.e.,

$$K(i,j)/K(j,i) = Q_j/Q_i \quad (2)$$

where the values of $K(i,j)$ are available in Ref. 5. The second and seventh term represent the population change caused by the spontaneous emission. The third term represents the recombination of ions with free electrons caused by three body collisions. The fourth term represents the change caused by bound-free transitions, including both spontaneous transitions as well as stimulated transitions. The reverse case of ionization from a bound to free state, i.e., photoionization, is included in the eighth term. The sixth term represents the bound-free transitions, again caused by electron collisions.

Solution of the master equation can be obtained by the integration of Eq. (1), which amounts to substantial numerical operations as well as the memory size. Fortunately, in the hypersonic environment of interest, we can assume the quasi-steady-state (QSS) condition. The QSS assumption is based on the fact that the rate of change of N_i on the left-hand side (LHS) of Eq. (1) is much smaller than both the sum of all incoming rates and sum of all outgoing rates on the RHS of Eq. (1):

$$\left|\frac{\partial N_i}{\partial t}\right| << \sum_{j=1}^{m} K(i, j)N_jN_e + \sum_{j=1}^{m} A(i, j)N_j + K(c, i)N^+N_eN_e + A(c, i)N_+N_e \tag{3}$$

$$\left|\frac{\partial N_i}{\partial t}\right| << \sum_{j=1}^{m} K(i, j)N_iN_e + K(i, c)N_iN_e + \sum_{j=1}^{m} A(i, j)N_i + A(i, c)N_i \tag{4}$$

Under this condition, the distribution of population can be determined by solving the set of algebraic equations resulting from setting the LHS of Eq. (1) to zero. This step should not be confused with the assumption of thermochemical equilibrium among the energy levels. To reduce the number of the algebraic equations, the electronic energy levels can be lumped into groups, some of which are approximately degenerate states. In the current study, the electronic energy levels are divided into 22 groups so that the 1st and 22nd group represent the ground state ($2P^3\ ^4S$) and the states close to the ionization limit, respectively. In Fig. 4, the population distribution of atomic nitrogen among electronic energy levels is shown. The x axis represents the group number of electronic states, whereas the y axis represents the number density of each group.

The most interesting fact is that the number densities of excited states decrease as the distance behind the shock increases, while the total number density of atomic nitrogen increases, which implies that a non-Boltzmann population distribution exists in the electronic energy levels. For the other atomic species, similar results can be obtained.

As in the case of atomic species, the number density distribution of molecular species can be calculated. In Fig. 5, the number density distribution of the electronic energy levels of molecular nitrogen is shown. Therein, the x axis represents the electronic energy level: the first level is $X^1\Sigma_g^+$, the second is $A^3\Sigma_u^+$, etc. For the calculation of the radiation, as explained in the next section, the electronic level population distribution of the other species (CN, NH, C_2, and N_2^+) were calculated but not shown for brevity.

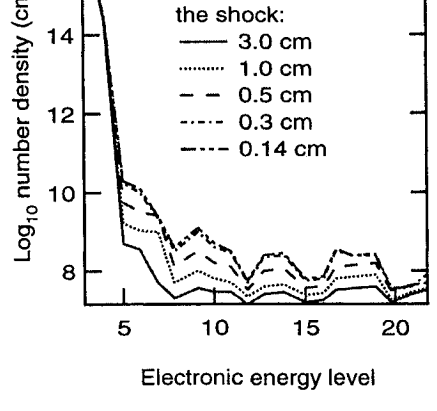

Fig. 4 Population distribution of atomic nitrogen among the grouped energy levels.

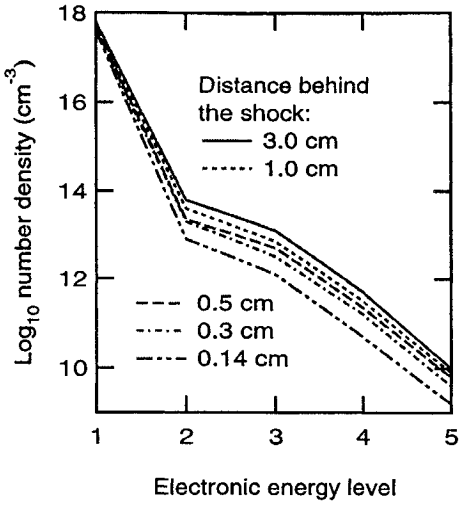

Fig. 5 Population distribution of molecular nitrogen among the electronic energy levels.

Radiation

Using the calculated number density distributions in the previous section, the radiation from the high-temperature gas was calculated by accounting for the contributions from all the individual rotational lines of molecules and atomic lines. The database of the NEQAIR code was modified for the calculation of the radiation from the species considered.

Atomic Radiation

To compute spectral intensities of a high-temperature gas, it is necessary to consider the interaction of the radiation with particles constituting the gas under consideration. If an optically thin, homogeneous gas is considered, I_λ can be expressed as[6]

$$I_\lambda = E_\lambda l \tag{5}$$

The starting point of the calculation is then to compute E_λ. Three different mechanisms for E_λ were considered. First, the bound–bound transitions were treated. Included were the line broadening mechanisms, namely, natural, pressure, Doppler, and Stark broadening. The widths from each broadening mechanism are well known and available from Ref. 7. Once the widths are calculated, the exact line shape of each atomic line can be determined by a convolution of the Gaussian and Lorentzian profile, which represents, respectively, Doppler and pressure broadening. Since this calculation takes a large computation time, an approximation of the convoluted line shape was used in the calculation as suggested in Ref. 6. Secondly, the bound-free transition was considered. This phenomenon corresponds to photoionization whose cross section has been calculated quantum mechanically with Gaunt factor as a parameter.[8] Thirdly, the free–free transition was considered, also called bremsstrahlung; this consists of photons emitted by free electrons accelerated by local electric fields. Using the absorption cross-sectional data in Ref. 9, the absorption was calculated, and the emission, which is the inverse process of absorption, was calculated by the principle of detailed balancing.

Molecular Radiation

The band spectrum of the molecular radiation includes the branches associated with the different types of electronic transitions.[10,11] In the current study, the calculation of the molecular

radiation was done following the same method used in Ref. 6. The line shape analysis was the same as for the atomic line broadening.

In Fig. 6, the calculated spontaneous emission spectrum of the gas located 1.5 mm behind the shock is shown. This is the location where the total radiation is most severe. To compare with the radiation at equilibrium, the spontaneous emission spectrum at 3 cm behind the shock is plotted in Fig. 7. As in Fig. 7, the magnitude of spontaneous emission at equilibrium is one order smaller than that at peak nonequilibrium.

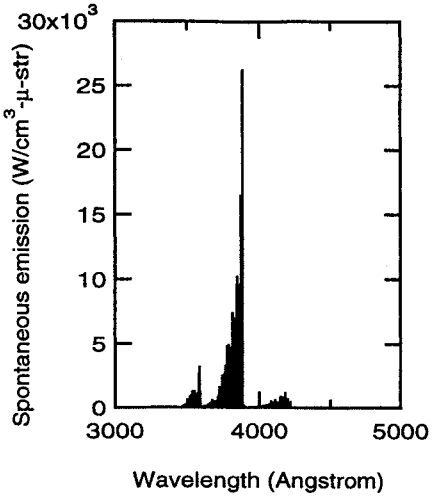

Fig. 6 Calculated spontaneous emission of gas 1.5 mm behind the shock.

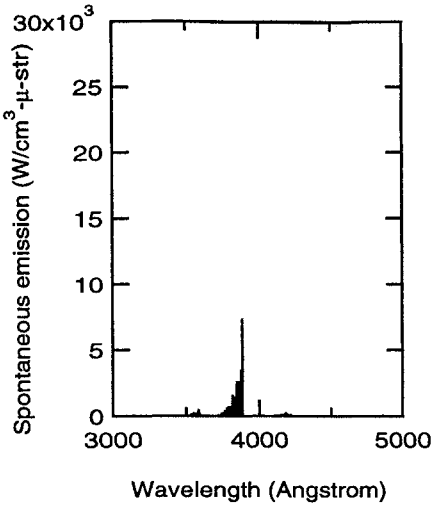

Fig. 7 Calculated spontaneous emission of gas at 3.0 cm behind the shock.

Experiments

To validate the computer codes used in the calculation of radiation in the previous section, the radiation from the high-temperature gas was measured. The primary measurement technique used was the optical diagnosis; photographic and photoelectric measurements. The high-temperature gas was generated by a combustion driven shock-tube facility and the schematic of the experimental setup is shown in Fig. 8. The shock tube used in this study is composed of two sections: 1) a 7.62-cm-in. i.d. cylindrical stainless-steel driving section and 2) a 5 × 5 cm^2 aluminum driven section. The driver section is filled with an 8:2:1 mixture of helium, hydrogen, and oxygen, which is ignited by spark plugs. Prior to the injection of test gas, the driven section, which is 3 m long, was not only wiped out with acetone and alcohol, but it was also baked by heating tapes up to 200°F to eject molecules stuck to the inside wall. During the baking process, a mechanical pump was operated first to give a rough vacuum followed by a cryopump to generate the high vacuum (10^{-6} torr).

Shock-generated radiation was observed through a test-section window. Quartz was used for the window material and flush mounted on the wall. The distance from the diaphram to the test section was 2.54 m, a location that yields the optimum test time.[12] Two photomultiplier tubes were used to measure the shock speed. In the current experiment, the accepted range of shock velocity was 5750 ± 150 m/s.

The detailed optical arrangement including a top view of the shock tube is shown schematically in Fig. 9. The light collected by a concave mirror is analyzed by a 1-m McPherson monochromator. As mentioned, two different types of experiments were possible by switching a mirror inside the monochromator. First, the whole spectrum of the gas can be captured by exposing a film to the one of exit slits of monochromator. Kodak tri-x pan film and high-speed infrared film were used to take the spectrum, which lasts a few microseconds. The developed films were analyzed in a densitometer at NASA Ames Research Center. By scanning the spectrum of the gas in the densitometer, one can obtain the wavelength as well as intensity, information that was used to identify the species present. Particular attention was paid to the CN band spectrum since CN was the strongest light emitter. Secondly, the absolute measurements of light intensity at selected wavelengths have been performed by using the exit slit on the other side of the monochromator and photomultiplier tube (Hamamatsu R105UH, R905) attached to that exit slit. The selected wavelengths are the centers of Voight profile of the identified atomic lines, or the center of molecular bands. The slit function of the monochromator was measured using a He–Ne laser and the measured full-width-of-half-maximum (FWHM) was 8.66 Å. As shown in Fig. 9, a spectral lamp (General Electric radiance

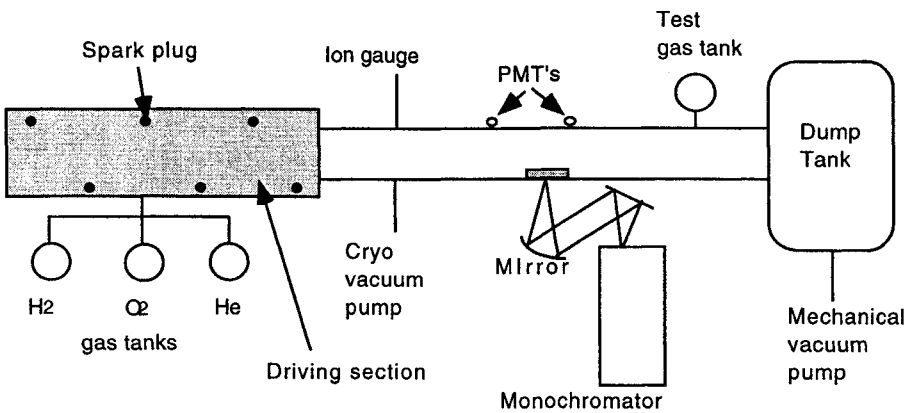

Fig. 8 Schematic diagram of the shock-tube configuration.

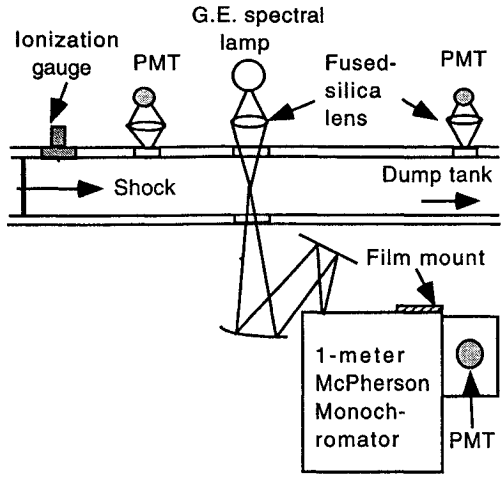

Fig. 9 Optical arrangement for the shock-tube experiments.

ribbon type tungsten filament) with a fused-silica lens was used to interpret the measurements in terms of absolute intensity.

In the current study, the experimental error originates from the uncertainty in data reduction and the scatter from several runs. To estimate the uncertainty in data reduction, the fluctuation of lamp emission and the uncertainty in focal length of the fused-silica lens because of chromatic aberration were measured. Measured values were compared with the numerical analysis and the results are discussed in the following sections.

Comparison of Results and Application

Comparison

The experimental data from the photomultiplier tubes for the absolute measurement of spontaneous emission spectrum were calibrated and shown in Fig. 10. The numerically calculated spontaneous emission spectrum was convoluted with the slit function of the monochromator to be compared with the experimental data. In Fig. 10, the dotted line represents the result from the numerical analysis. As can be seen, the absolute measurements of radiation at 3590 Å, which correspond to the CN violet 1–0 band center, show good agreement with numerical analysis. In Fig. 11, the convoluted spontaneous emission spectrum as a function of wavelength at a point that is located at 1.5 mm behind the shock is shown. The experimental data, represented as small circles, show good agreement with those of numerical analysis.

Based on the agreement in Figs. 10 and 11, the numerical code was applied to the analysis of two-dimensional wedge flow and to the calculation of the stagnation point heat flux on the Huygens probe, as discussed later.

Wedge Flow

In Fig. 12, a typical wedge flow is shown with several lines, which divide the flowfield into several slices. Since the flow properties in each slice are determined by the velocity component normal to the shock, the flow analysis can be carried out using the one-dimensional method mentioned in previous sections. Since the density of the flow in a slice increases as the flow marches further downstream, the height of each slice should be changed to satisfy the mass flux conservation. By accounting for all of the contributions from each slice, one can determine a new shock shape. One can then iterate on this procedure. A few iterations are enough to converge to a solution, as shown in Fig. 13. The freestream condition was chosen the same as the Titan atmospheric condition at 280 km altitude. The velocity was 8 km/s and the wedge angle was 45 deg. In Fig. 13, the dotted, heavier dashed, and solid line represent the shock of reacting gas, the shock of perfect gas, and wedge surface, respectively. Therein, the perfect gas represents

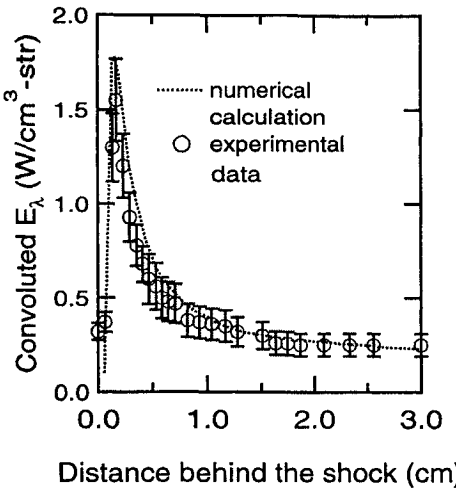

Fig. 10 Comparison of computed values with experimental data. The *y* axis is the convoluted spontaneous emission spectrum with slit function.

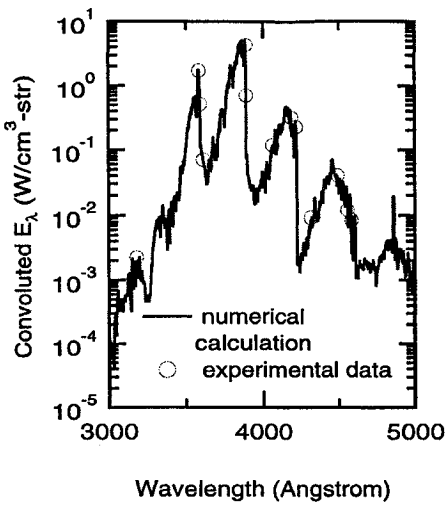

Fig. 11 Comparison of computed values with experimental data of which error is about ± 17% at 20:1 odds. The *y* axis is the convoluted spontaneous emission spectrum with slit function.

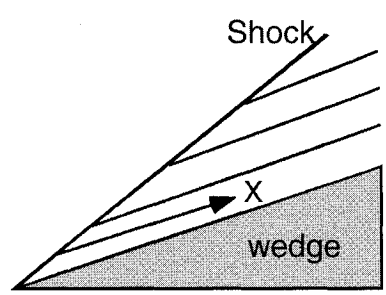

Fig. 12 Division of the flowfield into several regions for analysis.

a flow without chemical reaction, whereas the reacting gas represents the flow with the chemical reactions considered in the current analysis. As can be seen, the shock shape of reacting gas is the same as that of perfect gas near the apex of wedge and approaches that of equilibrium as the distance along the surface increases. From the shock shape, the pressure distribution along the surface can be calculated, which can be integrated to give C_L, C_D, and C_M. Under the flight conditions of Fig. 13, the C_L, C_D, and C_M of the ramp surface are 2.04, 1.72, and 0.0085, respectively. The most interesting fact is that pitching moment, which is an important factor for the stability, is not zero. The origin of pitching moment in early re-entry

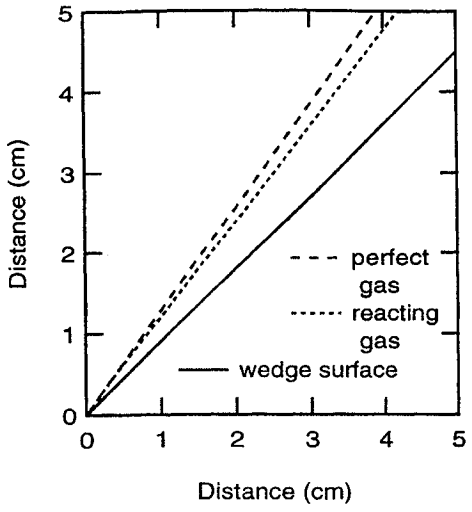

Fig. 13 Shock waves on a two-dimensional wedge.

flights data, such as Apollo and the Space Shuttle, was studied by several authors and summarized in Ref. 5. Therein, it is believed that the real gas effect is one of the main sources of pitching moment.

Stagnation Point Heat Flux

The basic aim of this study is the estimation of the effect of nonequilibrium shock-layer radiation on the stagnation point heat flux. The freestream condition was chosen the same as the Titan atmospheric condition at 280 km altitude. The freestream density, temperature, and velocity are 2.62×10^{-4} kg/m^3, 183 K, and 4.75 km/s, respectively. Since the numerical solution of the axisymmetric flow is quite complicated, one assumption was made: the emission in the flowfield at an arbitrary point can be determined from the one-dimensional flow behind the normal shock if the particle times to the point are the same. This is explained in Fig. 14. To calculate the particle time in the shock layer, the flow velocity in the shock layer should be calculated. As suggested in Ref. 13, the governing equations for the shock-layer flow were integrated using a coordinate transformation. The shock standoff distance can be obtained from that solution and the distance was 8.9 cm in this flight condition. This value was used to determine the particle flow time in the shock layer, and thus the radiation field. The total spontaneous emission $E(y)$, defined as

$$E(y) = \int_0^\infty E_\lambda(y)\, d\lambda \tag{6}$$

was calculated along the stagnation streamline and is shown in Fig. 15. From this distribution, the radiative heat flux on the stagnation point Q_r can be calculated by

$$Q_r = \frac{\int_0^\delta E(y)\, dy}{2} \tag{7}$$

The radiative heating on the stagnation point was found to be 11.6 W/cm^2 at the selected flight condition. A similar work has been done by Nelson et al.,[14] who estimated radiative heat flux to be 16.2 W/cm^2 at the same flight condition with a different atmospheric gas mixture. Based on the method in Ref. 15, the corresponding convective heat flux was approximately 30 W/cm^2, which means that the nonequilibrium radiative heat flux was more than 25% of the total heat flux. The equilibrium radiative heat flux is roughly an order of magnitude smaller.

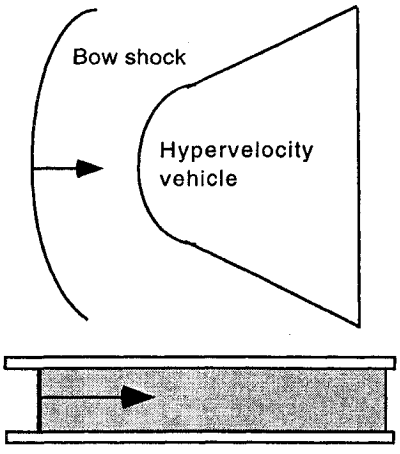

Fig. 14 Schematic showing the correspondence between the flow along stagnation streamline and the flow in a shock tube.

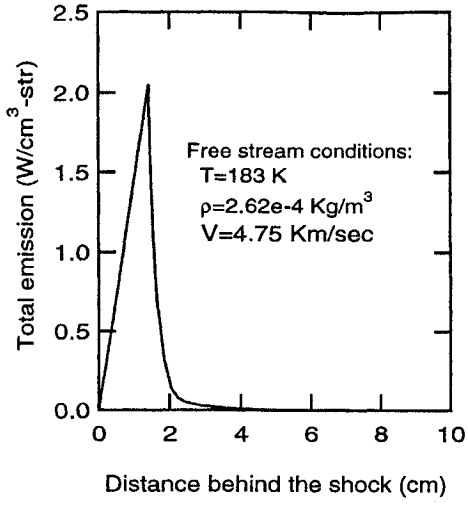

Fig. 15 Total emission as a function of the distance behind the shock.

Conclusions

The major conclusions of this study are the following:

1) The three-temperature model is an appropriate one for computing the nonequilibrium thermochemical and radiative behavior in the shock layer of a hypersonic vehicle penetrating the Titan atmosphere.

2) The nonequilibrium behavior produces a large overshoot in radiative emission closely behind the shock, which decreases to the equilibrium value, defining a radiation relaxation zone.

3) The total nonequilibrium shock-layer radiation is about an order of magnitude larger than that generated by an equivalent equilibrium flow.

4) Radiation from the nonequilibrium flow produces a significant surface heat transfer. It cannot be neglected relative to the convective heat transfer.

5) Calculation of aerodynamic coefficients shows that nonequilibrium flow changes the location of the c.p., which produces a finite nose-up pitching moment and can lower the vehicle's stability against tumbling.

References

[1]Park, C., "Radiation Enhancement by Nonequilibrium During Flight Through the Titan Atmosphere," AIAA Paper 82-0878, June 1982.

[2]Park, C., "Nonequilibrium Air Radiation Program: User's Manual," NASA TM 86707, July 1985.

[3]Park, C. S., and Bershader, D., "Determination of the Radiative Emission of a Hypersonic Flow Simulating the Cassini-Titan Atmospheric Entry Probe Environment," AIAA Paper 90-1558, June 1990.

[4]Park, C. S., "Studies of Radiative Emission from the Simulated Shock Layer of the Huygens Probe," Ph.D. Dissertation, Stanford Univ., Stanford, CA, 1991.

[5]Park, C., *Nonequilibrium Hypersonic Aerodynamics*, 1st ed., Wiley, New York, 1990, pp. 85–88.

[6]Arnold, J. O., Whitting, E. E., and Lyle, G. C., "Line by Line Calculation of Spectra from Diatomic Molecules and Atoms Assuming a Voigt Profile," *Journal of Quantitative Spectroscopy and Radiative Transfer*, Vol. 9, No. 6, 1969, pp. 775–798.

[7]Seigman, A. E., *Lasers*, 1st ed., Univ. Science Books, Mill Valley, CA, 1986, pp. 157–175.

[8]Griem, H., *Plasma Spectroscopy*, 2nd ed., McGraw-Hill, New York, 1964, Chaps. 3–5.

[9]Peach, G., "Continuous Absorption Coefficients for Non-Hydrogenic Atoms," *Memoirs of the Royal Astronomical Society*, Vol. 73, Pt. 1,1970, pp. 1–123.

[10]Banwell, C. N., *Fundamentals of Molecular Spectroscopy*, 1st ed., McGraw-Hill, New York, 1986, pp. 40–154.

[11]Herzberg, G., *Molecular Spectra and MolecuSpectra of Diatomic Molecules*, 2nd ed., Van Nostrand, New York, 1950, pp. 1–280.

[12]Camm, J. C., and Rose, P. H., "Electric Shock Tube for High Velocity Simulation," Avco Everett Research Lab., Research Rept. 136, July 1962.

[13]Park, C., "Dissociative Relaxation in Viscous Hypersonic Shock Layer," *AIAA Journal*, Vol. 2, No. 7, 1964, pp. 1202–1207.

[14]Nelson, H. F., Park, C., and Whiting, E. E., "Titan Atmospheric Composition by Hypersonic Shock Layer Analysis," *Journal of Thermophysics and Heat Transfer*, Vol. 5, No. 2, 1991, pp. 157–165; also AIAA Paper 89-1770, June 1989.

[15]Fay, J., and Riddle, F., "Theory of Stagnation Point Heat Transfer in Dissociated Air," *Journal of Aeronautical Science*, Vol. 25, No. 2, 1968, pp. 73–85.